**TABLE S1, related to Figure 3.** Mitochondrial Respiration Rates with Different Substrates

| ***Liver Mitochondria*** | ***Wild-Type*** | ***CD38KO*** |
|---|---|---|
| ***Glutamate*** | | |
| *State II* | 28.3 ± 9.4 | 53.6 ± 12.1* |
| *State III* | 121.6 ± 19 | 209 ± 18* |
| *State IV* | 38.3 ± 9.8 | 60 ± 16* |
| *Uncoupled* | 127.3 ± 25 | 202 ± 4.2* |
| ***Palmytoil-Carnitine +Malate*** | | |
| *State II* | 54.5 ± 13 | 77 ± 28* |
| *State III* | 91.5 ± 21 | 121 ± 24* |
| *State IV* | 42.5 ± 10 | 53 ± 98* |
| *Uncoupled* | 102 ± 15 | 140 ± 18 |

**TABLE S2, related to Figure 3.** Spleen Mitochondrial Respiration Rates

| ***Spleen Mitochondria*** | ***Wild-Type*** | ***CD38KO*** |
|---|---|---|
| ***Succinate+Rotenone*** | | |
| *State II* | 127 ± 2.8 | 304 ± 105* |
| *State III* | 223 ± 47 | 456 ± 145 |
| *State IV* | 54 ± 6.3 | 104 ± 12* |
| *Uncoupled* | 197 ± 71 | 534± 194* |

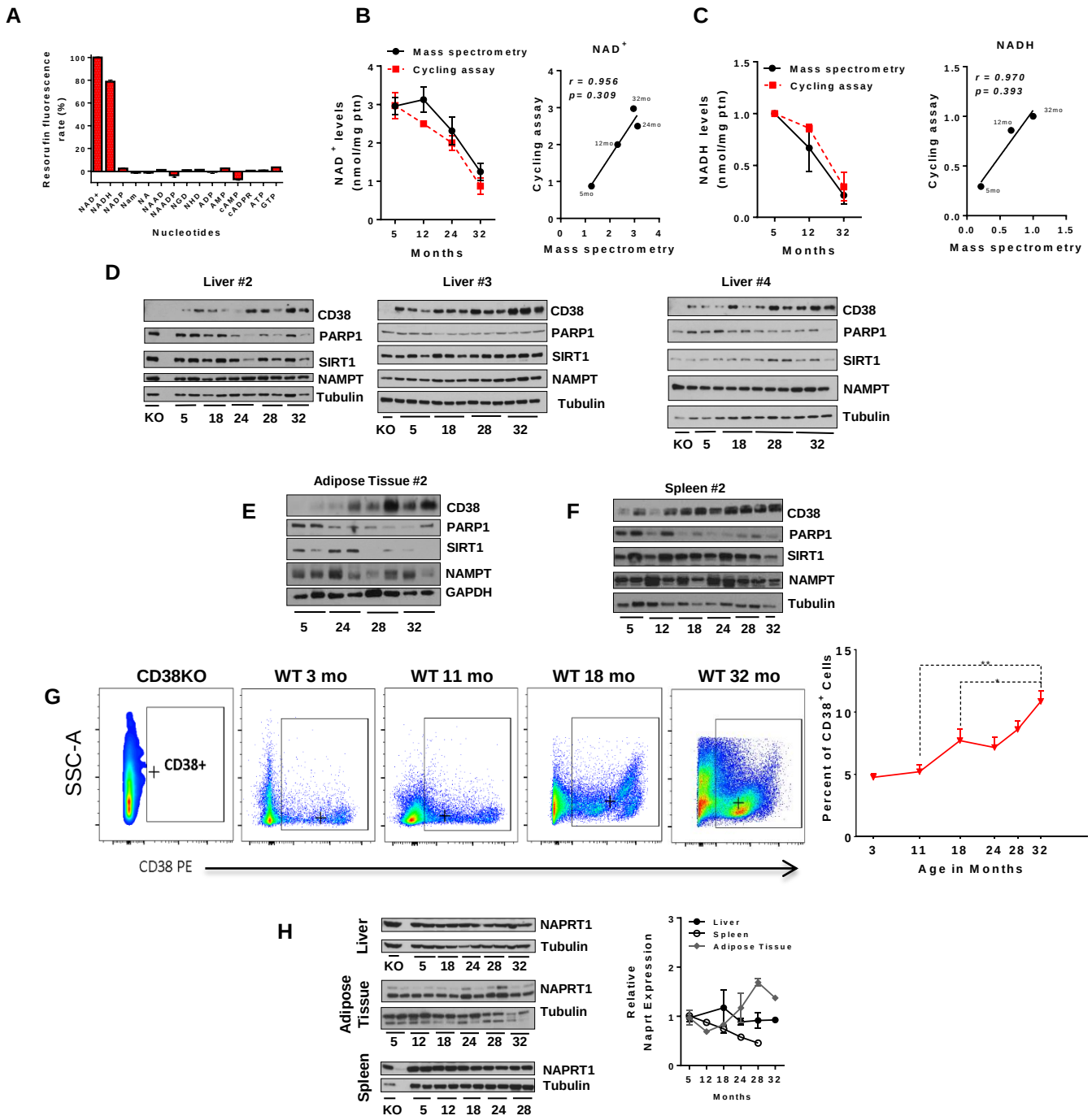


**Figure S1, related to Figure 1**. **(A)** Resorufin fluorescence rate using the alcohol dehydrogenase reaction. Experimental conditions were the same for all nucleotides (50nM). Results are means ± S.E from three independent measurements, normalized against NAD+ levels. **(B)** Total $NAD^+$ levels in WT and CD38KO mice liver tissue during aging measured by two methods: mass spectroscopy (black line) and cycling assay (red dotted line), (n=4). The Pearson correlation coefficient (r) was: r = 0.956. **(C)** NADH levels in WT and CD38KO mice liver tissue during aging measured by two methods: mass spectroscopy (black line) and cycling assay (red dotted line), (n=4). The Pearson correlation coefficient (r) was: r = 0.970. **(D-F)** Immunoblots for CD38, NAMPT, PARP1, and SIRT1 in liver **(D)**, adipose tissue **(E)** and spleen **(F)** of mice in different ages. **(G)** Flow cytometric assessment of CD38+ cells in mouse liver with aging. Representative flow plots showing analysis of CD38+ population in liver of CD38KO (negative control) and C57BL6 mice at 3, 11, 18, and 32 months of age; graph shows mean ± SEM for n=4 mice per age (*p<0.05, **p<0.01 versus 11 mo. old). **(H)** Immunoblots for NAPRT1 in liver, adipose tissue and spleen of mice in different ages. On the right, graph shows mean + SEM of relative protein expression of NAPRT1. Relative expression of the protein was calculated to Tubulin in each lane and then calculated relative to 5 month old mice (*p<0.05).

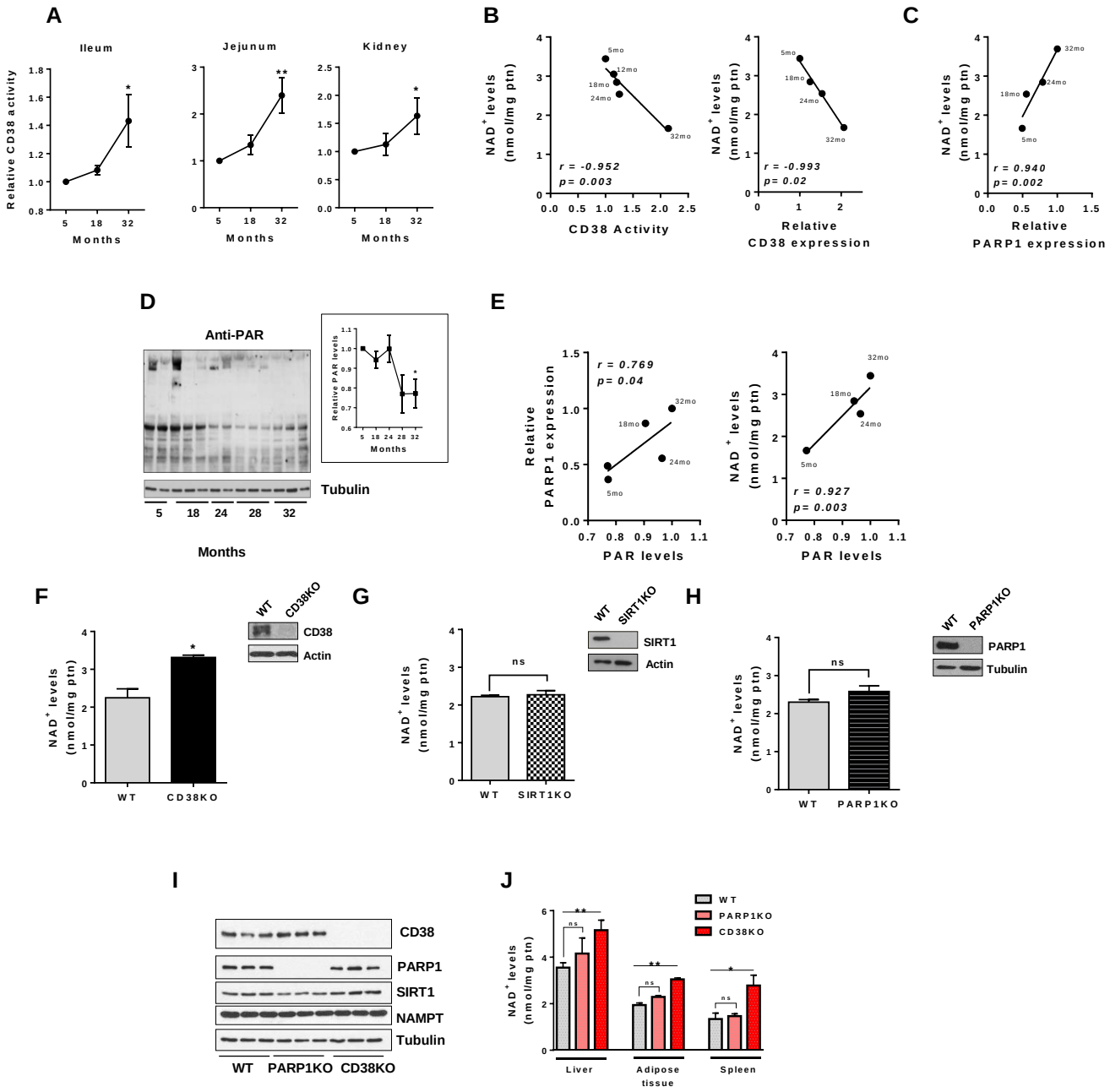


**Figure S2, related to Figure 2** . **(A)** CD38 activity in ileum, jejunum and kidney of mice of different ages (n=4, *p<0.05 versus 5 month old mice). **(B)** $NAD^+$ levels of aging mice liver tissue are plotted against relative CD38 activity or CD38 protein expression. The Pearson correlation coefficient (r) was significant in both cases: r = −0.95, p= 0.003 and r=-0.99, p= 0.02, respectively. **(C)** Pearson correlation coefficient (r) and corresponding p-value between $NAD^+$ levels of aging mice liver tissue and the relative PARP1 protein expression is displayed. **(D)** Immunoblots for PAR and Tubulin in mice liver tissue (left). On the right, graph shows relative protein expression of PAR, calculated as a ratio to Tubulin in each lane, and then calculated relative to 5 month old mice (n=3, *p<0.05). **(E)** PAR levels of aging mice liver tissue are plotted against relative PARP1 protein expression and $NAD^+$ levels. The Pearson correlation coefficient (r) was significant in both cases: r = 0.769, p= 0.04 and r= 0.927, p= 0.003, respectively. **(F-H)** NAD+ levels in primary mouse embryonic fibroblasts (MEFs) purified and cultured from wild-type (WT), CD38 knockout (F), SIRT1 knockout (G), and PARP1 knockout (H) mice (n=5, **p<0.001, ns=non-significant (p>0.05) versus WT). **(I)** Immunoblots for CD38, NAMPT, PARP1, SIRT1 and Tubulin in liver of WT, PARP1KO and CD38KO mice, each lane shows one independent mouse. **(J)** $NAD^+$ levels in liver, adipose tissue and spleen of WT, PARP1KO and CD38KO mice (n=4, *p<0.05, **p<0.001, ns=non-significant (p>0.05).

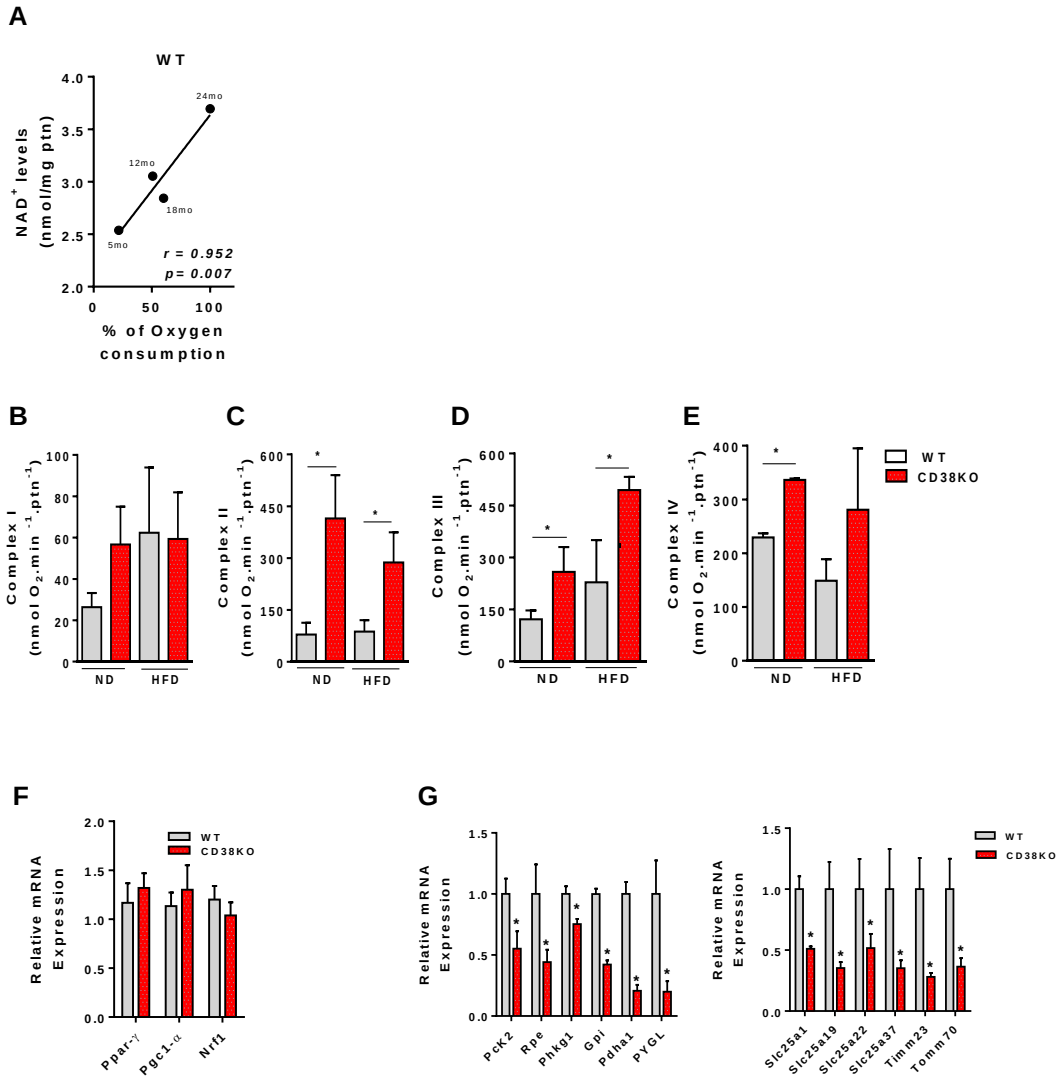


**Figure S3, related to Figure 3. (A)** Correlation between age-related decrease in $NAD^+$ levels and mitochondrial function. NAD+ levels of aging WT mice liver tissue are plotted against the percentage of oxygen consumption. The Pearson correlation coefficient (r) is significant: r = 0.952, p= 0.007. **(B-E)** Mitochondrial complex I (NADH:Ubiquinol oxireductase) activity **(B)**, complex II activity **(C)**, complex III activity **(D)** and complex VI activity **(E)** measured in intact mitochondria isolated from two year old litter mate WT and CD38 KO mice submitted to 16 weeks of normal (ND) or high fat diet, 42% of fat (HFD). (n=5, * p <0.05 versus WT mice, normal diet). **(F)** Relative mRNA expression of genes related to mitochondria biogenesis in liver from one year old WT and CD38KO mice. (n=4, * p <0.05 versus WT mice). **(G)** Relative mRNA expression in liver from one year old CD38KO mice compared to WT. The genes encoded the related proteins: *Pck2* (mitochondrial phosphoenolpyruvate carboxykinase (GTP) family), *Rpe* (ribulose-5-phosphate-epimerase), *PhgK1* (pyruvate kinase subunit – glycogenolytic regulatory enzyme), *Gpi* (phosphoglucose isomerase), *Pdha1* (pyruvate dehydrogenase subunit E1 alpha1), *Pygl* (liver glycogen phosphorylase), *Slc25a1* (mitochondrial citrate transport protein, CTP), *Slc25a19* (mitochondrial thiamine pyrophosphate carrier), *Slc25a22* (mitochondrial glutamate carrier), *Slc25a37* (mitochondrial iron transporter), *Timm23* (mitochondrial import inner membrane translocase subunit), *Tomm70* (translocase of outer mitochondrial membrane 70 homolog A (S. cerevisiae)). (n=4, *p<0.05 versus WT mice)

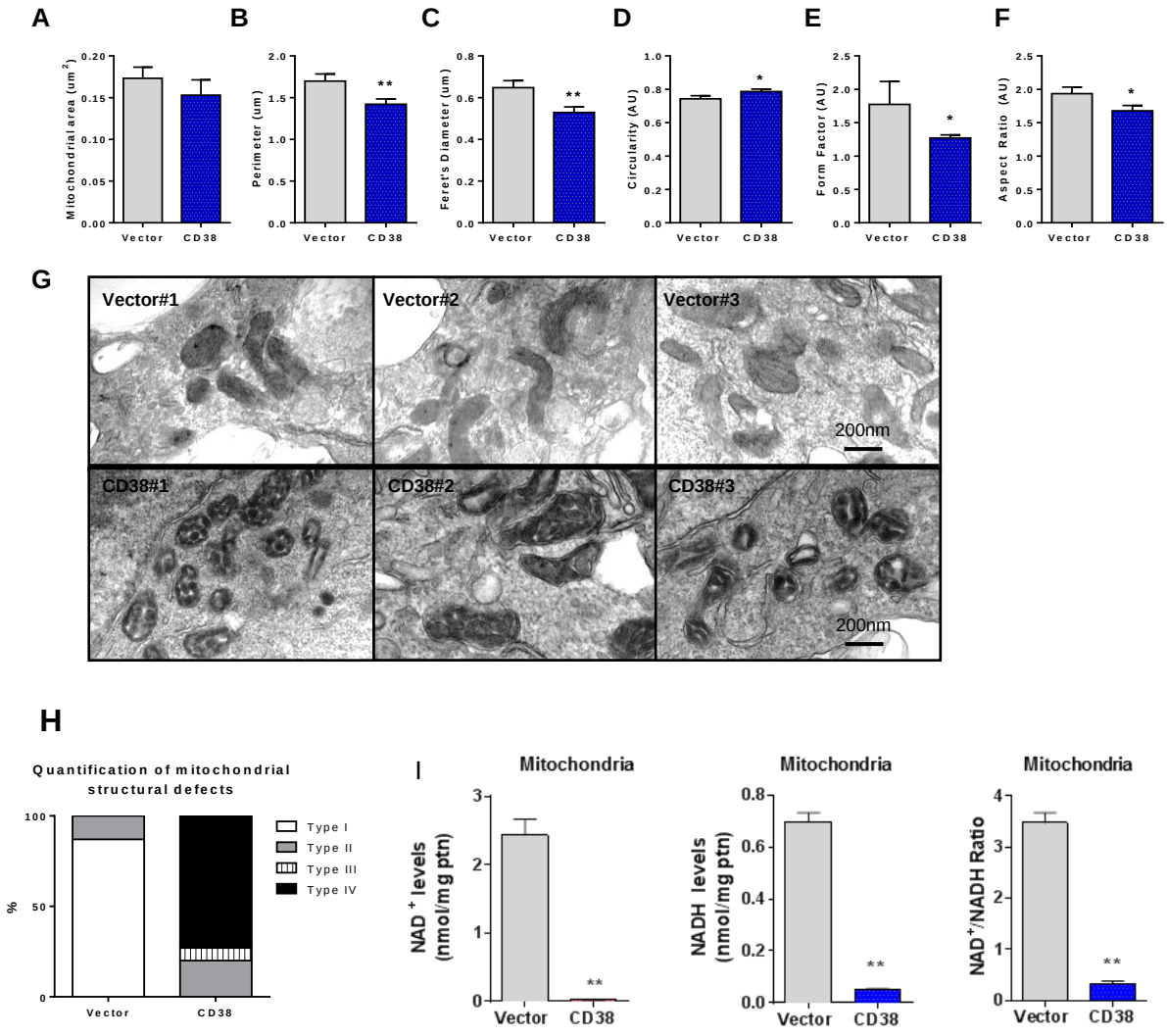


**Figure S4, related to Figure 4**. **Effects of CD38 overexpression in mitochondrial morphology. (A-F)** Mitochondrial size parameters: area **(A)**, perimeter **(B)**, and Feret's diameter **(C)**. Mitochondrial shape descriptors : circularity **(D),** form factor **(E)** and aspect ratio **(F)**. (A-F) $n$ =48 control mitochondria and $n$=64 CD38 mitochondria from 3 different experiments. Mean ± SEM. (*AU* arbitrary units); $*p < 0.05$, $**p < 0.01$. **(G)** Transmission Electron Microscopy (TEM) in cells transfected with empty vector (upper panel) or CD38 (lower panel). The scale bar is 200 nm for all three independent experiments in each group shown in the figure. **(H)** Quantification of mitochondrial ultrastructural defects. Blinded subjects were asked to score TEM images based on a score described in the methods section. Percentages of TEM images with intact mitochondria with normal appearing cristae (Type I); abnormal mitochondria with either swollen, irregular or whorling cristae (Type II); mitochondria with discontinuous outer membrane or deficient cristae (Type III); and mitochondria with both swollen and deficient cristae or both discontinues outer membrane and swollen cristae (Type IV) have been expressed from a total pool of 8 independent TEM pictures of each group presented to the subjects. **(I)** Mitochondria were isolated from cells transfected with empty vector (gray) or CD38 (blue). After isolation content of nucleotides were measured by cycling assay n=4, $**p < 0.01$.

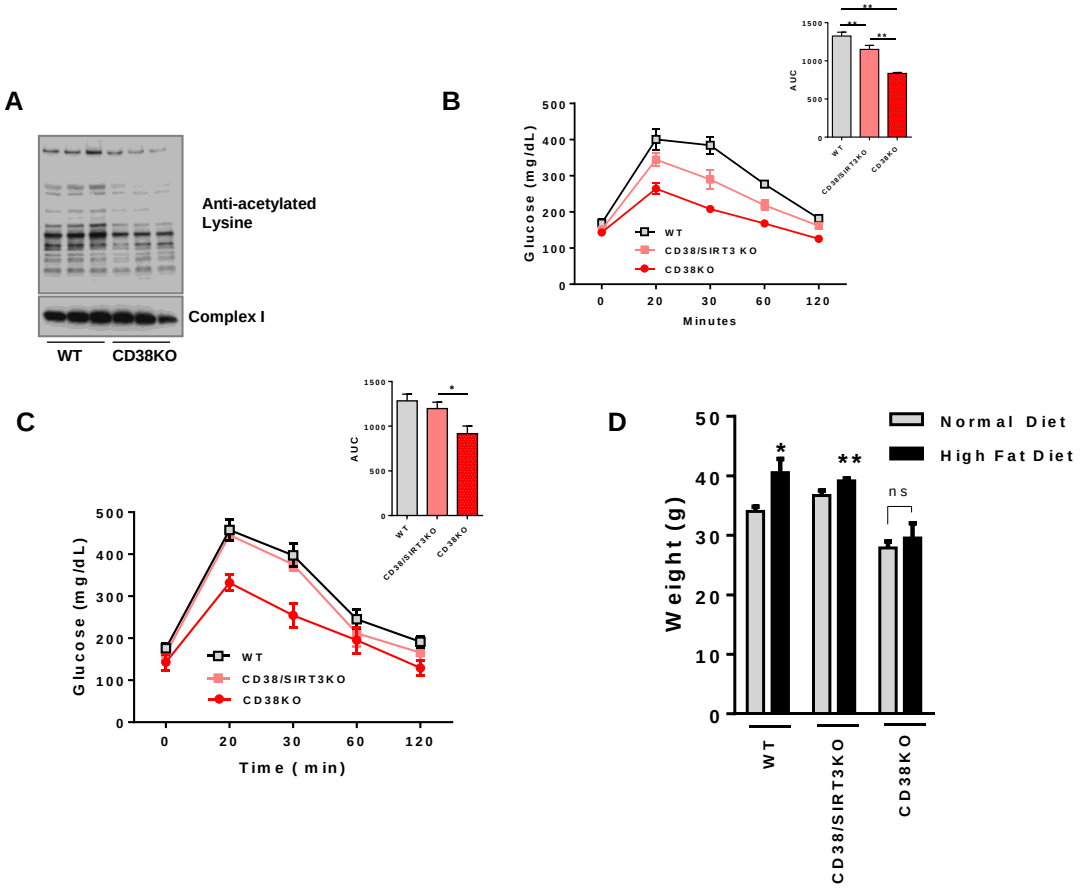


**Figure S5, related to Figure 5. (A)** Mitochondrial protein acetylation profile from six different mice than in figure 5 mice were one year old. **(B)** Glucose concentration in one year old WT, CD38/SIRT3KO and CD38KO mice in normal chow. Inset: Area under the curve from experiments (n=10, * p <0.05 versus WT mice). **(C)** Glucose concentration in one year old WT, CD38/SIRT3KO and CD38KO mice after 16 weeks of high fat diet. Inset: Area under the curve from experiments (n=10, * p <0.05 versus WT mice). **(D)** Body weight of one year old mice on normal chow diet and after 16 weeks of high fat diet (n=10, * p <0.05 versus mice in normal diet). The mice in B-C were one year old at the beginning of the study.

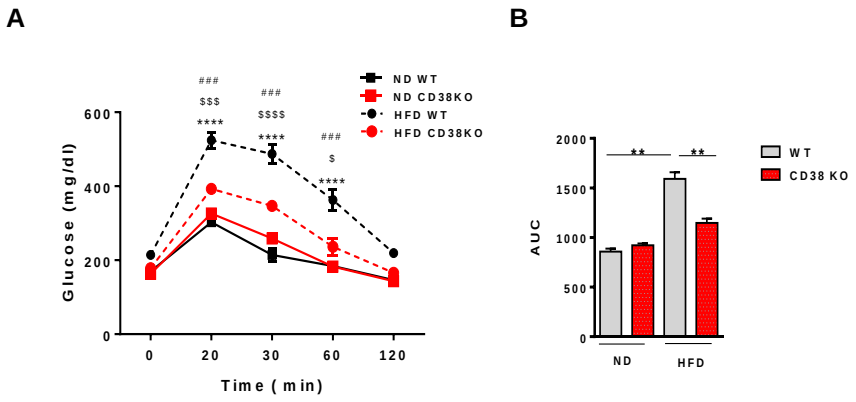


**Figure S6, related to Figure 6. (A)** Glucose concentration in 24 month old WT and CD38KO mice after intraperitoneal injection of glucose. Experiments made before and after 16 weeks of high fat diet. Area under the curve for glucose concentrations in different mice (**p<0.01, n=10). Data are expressed as means±SE. **(B)**. Two-way ANOVA and Bonferroni's post-test with repeated measures show significant interaction between the glucose curve for HFD WT and HFD CD38KO (****p<0.001*); ND CD38KO and HFD CD38KO (*$ p<0.05, $$$ p<0.001, $$$$ p<0.0001*); and ND WT and HFD WT (*### p<0.001*).

## SUPPLEMENTAL EXPERIMENTAL PROCEDURES

### Animal Studies

CD38/SIRT3 double KO mice (Figure 5) were generated by crossing CD38KO mice (C57BL/6 background) with SIRT3KO mice (129S background) to produce double heterozygous mice. These mice were then crossed, and the offspring genotyped for CD38 and SIRT3 mutations by PCR. CD38 primers were: oIMR0092 (*5'-AAT CCA TCT TGT TCA ATG GCC GAT C-3'*), oIMR7727 (*5'-CAC CAT AAG AGG GGA AGC AA-3'*), and oIMR7728 (*5'-TGC CAA AAG TGC AGA AGA GA-3'*). SIRT-3 primers were: SIRT3-KO -1*(5'-CTT CTG CGC CTC TAT ACA CAG-3'),* SIRT3-KO-2 *(5-TGC AAC AAG GCT TTA TCT TCC-3')* and SIRT3-KO-3*(5'-TAC TGA ATA TCA GTG GGA ACG-3').* PCR products were separated by agarose gel electrophoresis and visualized by ethidium bromide staining. After three crosses of the heterozygous the F3 generation was used for the generation of the animals used for the our experiments. CD38KO animals that were wild type or knockout for SIRT3 were used for experiments. Importantly, all mice used in the double knockout studies (non-mutant, CD38 single mutant and CD38/SIRT3 double mutant) were on a mixed C57BL6/129S background (the mixed background was present only on the animals used for the experiments of figure 5. All other wild type and CD38 KO mice were on a pure C57BL6 background. The experiments presented in figure 1 were performed with wild type animals from the aging NIA animal colony (CD38 KO tissues were used in these experiments to demonstrate the specificity of the CD38 antibody used). The same results as presented in figure 1, namely increase in CD38 expression with aging, were also observed when we assayed the same parameters in our own wild type mice that were generated by heterozygous cross of our CD38 colony. Except for figure 1 and figure 5, in all other animal experiments the comparison is made between wild type and CD38 KO litter mates in a pure C57BL6 background. Mice were maintained on a normal chow diet (ND) (PicoLab 5053 Rodent Diet 20; Lab Diets) *ad libitum,* except when the High-fat diet (HFD is indicated.

For high-fat diet (HFD) experiment, mice received a diet containing 42% of calories from fat (TD.88137, Harlan Laboratories, Inc., Indianapolis, IN) for 16 weeks. A single dose of NR (ChromaDex) 500mg/kg body weight was then administered by intraperitoneal (i.p.) injection. Control mice received vehicle (saline) injections. Directly following injection, mice were fasted for 15 hours for assessment of fasted glucose levels and glucose tolerance (GTT). For GTTs, blood was collected

from the tail vein before and 15, 30, 60, and 120 min after i.p. injection of 50% dextrose (1.5g/kg body weight). Blood glucose levels were measured using an AlphaTrak II glucometer (Abbott Laboratories).

For measurements of NR, NMN, $NAD^+$, and NAM content in blood, mice were fasted overnight before NR (500 mg/kg, i.p.) was administered. Blood was collected from the tail vein at 0-150 min, and 20% trichloroacetic acid (TCA) was added to stop reaction. After extraction by organic solvent, the nucleotide content was determined by HPLC.

**Cell Culture**

HEK293T and MEFs were cultured in DMEM with 10% FBS, and penicillin/streptomycin (Life Technologies). A549 cells were cultured in RPMI with 10% FBS and penicillin/streptomycin (Life Technologies). Transfections with Flag or Flag-CD38 vector were performed using Lipofectamine 2000 (Life Technologies) and 5μg of total DNA in media without antibiotics. Experiments were performed 48h after transfection.

**Electron Microscopy and quantification of mitochondria morphology parameters**

Measurements were generated from transmission electron microscopy images with a magnification of ×20,000. Image J software (version 1.42q, National Institutes of Health, Bethesda, MD) was used to calculate all the mitochondrial size and shape parameters by drawing around of each individual mitochondrion analyzed (Picard, et al., 2010). Surface area (mitochondrial size) is reported in squared micrometers; perimeter in micrometers; aspect ratio (AR) is computed as [(major axis)/(minor axis)] and reflects the "length-to-width ratio"; form factor (FF) [(perimeter2)/(4π·surface area)] reflects the complexity and branching aspect of mitochondria; circularity [4π·(surface area/perimeter2)] is one two-dimensional index of sphericity with values of 1 indicating perfect spheroids; and Feret's diameter represents the longest distance (μm) between any two points within a given mitochondrion. Quantification of mitochondrial ultrastructural defects was done by blinded subjects who were asked to classify TEM images based on a score described by Sisková, et al. 2010. Percentages of TEM images with intact mitochondria with normal appearing cristae (Type I); abnormal mitochondria with either swollen, irregular or whorling cristae (Type II); mitochondria with discontinuous outer membrane or deficient cristae (Type III); and mitochondria with both swollen and

deficient cristae or both discontinues outer membrane and swollen cristae (Type IV) have been expressed from a total pool of 8 independent TEM pictures of each group presented to the subjects.

**Flow Cytometry**

Mouse liver tissue was minced and digested with liberase (Sigma) at 37° C for 15 minutes to make single cell suspensions. Cells were incubated with FC-receptor block (Miltenyi), stained with anti-mouse CD38-PE and Ter119-APC/Cy7 antibodies (Biolegend) for 45 min at 4° C, and subjected to flow cytometry on BD LSRII (BD Biosciences). Zombie NIR dye (Biolegend) was used to discriminate live/dead cells. Data were analyzed with FlowJo software (FlowJo, LLC) using the following gating strategy: 1) erythrocytes ($Ter119^+$) and dead cells were excluded; 2) doublets (FSC-H vs. FSC-A) and debris (SSC-A vs. FSC-A) were excluded; and 3) $CD38^+$ cells were gated (SSC-A vs. CD38-PE).

**NAD/NADH UPLC-Mass Spectrometry Method**

*Instrumentation:* The LC-MS system consisted of a Waters Aquity H class ultra-performance liquid chromatography (UPLC) system, containing a quaternary solvent manager and sample manager-FTN coupled to a Xevo TQ-S mass spectrometer (Waters, Milford, MA) equipped with an electrospray ionization (ESI) source. Data was acquired and analyzed by Waters MassLynx v4.1 software.

*Chromatographic conditions*: The liquid chromatographic separation of NADH and $NAD^+$ was accomplished using an Agilent Poroshell 120 EC-C18 pre-column (2.1x5mm, 2.7µ, Chrom Tech, Apple Valley, MN) attached to an Agilent Poroshell 120 EC-C18 analytical column (2.1x100mm, 2.7 µm Chrom Tech, Apple Valley, MN) at 40°C, eluted with a gradient mobile phase composed of water with 0.1% formic acid (A) and ACN with 0.1% formic acid (B) with a constant flow rate of 0.5 mL/min and a total run time of 10 min. The elution was initiated at 100% A and held for 2 min, then B was linearly increased from 0-60% B for 4 min, 60% B was held for 1 min, and returned to initial conditions in .2 min, finishing with 2.8 min at 100% A. Auto-sampler temperature was 4°C and sample injection volume was 10 µl. $NAD^+$ and NADH were eluted at 1.6 and 3.5 minutes respectively. In control experiments we observed that none of the other NAD related metabolites (including NADP, NADPH, ATP, NAADP, NAAD, ADP, cADPR, ADPR, nicotinamide and nicotinic acid co-eluted with either $NAD^+$ or NADH.

Detection of $NAD^+$ and NADH were accomplished using the mass spectrometer in positive ESI mode using capillary voltage 3.5 kV, source temp 150°C, desolvation temp 500°C, cone gas flow 150 L/hr, desolvation gas flow 500 L/hr, using multiple reaction monitoring (MRM) scan mode with a dwell time of 0.075 sec. The cone voltages and collision energies were determined by MassLynx-Intellistart, v4.1, software. Values are as follows:

$NAD^+$ – m/z 664.27>136.09 - cone voltage 54V --- Collision 42 eV

NADH – m/z 666.28>514.17 – cone voltage 56V --- Collision 26 eV

N- Cyclohexyl benzamide – m/z 204.1>122.00 – Cone voltage 80 V – Collision 20 eV

*Stock solution preparation:* The primary stock solutions were prepared in silanized glass vials as follows: $NAD^+$ (10 mg/ml in water) and NADH (1 mg/ml in .01 N NaOH, pH 11.9) n-Cyclohexyl benzamide (IS) (100 ug/ml in EtOH) all were stored at -80°C. Working standards were prepared by dilution of the stock solution into the same solutions mentioned above. Daily standard samples were prepared by diluting above stocks 1:20 in water containing 500-ng/ml internal standard.

Mouse tissue samples were prepared as described in the method section. Samples were thawed on ice. Samples were diluted in water containing 500 ng/ml of internal standard. Samples for $NAD^+$ measurement were diluted 1:1000 and 1:10000, whereas the ones for NADH samples were diluted 1:1000 in slick microfuge tubes. Samples were vortexed and transferred to 2 ml auto-sampler vials for immediate analysis.

**NR, NAD+ and NMN Measurements by HPLC**

Blood from WT and CD38KO mice after NR or vehicle treatment was collected and extracted by organic solvent and neutralized by NaOH on ice. For measurements, the HPLC was at a flow rate of 0.25 ml/min with 99% buffer A from 0-3 min, a linear gradient to 99% buffer A/1% buffer B (100% methanol) from 3-20 min, 80% buffer A/20% buffer B from 20-21 min, a linear gradient to 30% buffer A/70% buffer B from 21-28 min at 0.35 ml/min, 99% buffer A/1% buffer B from 28-31 min, and a linear gradient to 99% buffer A from 31-37 min at 0.25 mL/min. The protocol was adjusted based on previous studies (Yoshino & Imai, 2013). Concentrations were quantitated based on the peak area compared to a standard curve and normalized to volume of blood collected.

**Mitochondria Isolation**

After removing the tissue as described in the manuscript, the homogenates were centrifuged at 600 *x g* for 5 min. The supernatant was removed and centrifuged at 7000 *x g* for 10 min. The pellet obtained from spleen was resuspended in the buffer and centrifuged one more time at 7000 *x g* for 10 min. The final spleen pellet was resuspended in respiration buffer (MIR05, described below) for respiration measurements or frozen for other experiments. The pellet obtained from liver was resuspended in isolation buffer containing 15% of percoll (Invitrogen). A percoll gradient was placed in a centrifugation tube starting with isolation buffer containing 40% percoll in the bottom, followed by 22% percoll and 15% percoll at the top containing the pellet. The tube was centrifuged at 25,000 *x g* for 5 min. After the centrifugation, a percoll gradient is formed inside the tube and purified liver mitochondria fraction is placed between the two lower layers. The fraction is removed carefully and resuspended in isolation buffer. Two more centrifugations at 7000 *x g* for 10 min were done to wash out percoll from the sample. The final liver mitochondria pellet was resuspended in MIR05 + BSA fatty acid free 1mg/mL for respiration experiments or frozen for other experiments. Final protein concentration was between 10-15 mg/mL. With this isolation method our mitochondria preparation show an average respiratory control ratio, RCR (state $3^{ADP}$/ state 4) of 3.5±0.5.

**Mitochondrial Function**

*Cells* - Cells were washed with PBS, trypsinized and resuspended in culture medium without serum. 1-5 x $10^6$ cells were added in oxygraph chamber at the same time right before closing the chambers. The basal respiration rate was detected (*routine respiration*) after 15 minutes of oxygen consumption in culture media, oligomycin (2 μg/mL) was added to inhibit ATP synthesis (*leak respiration*), followed by a carefully titration with FCCP (0.2-2.5 mM) until a maximum electron transport capacity was reached (*ETC*). Rotenone (2 μM) + antimycin A (2.5 μM) were added to inhibit mitochondrial respiration and the residual oxygen consumption rate, which was not mitochondria-related, was subtracted from all the other respiration measurements. The respiration coupled to ATP production was calculated by the difference between routine and leak respirations rates (*couple respiration*) (Brand & Nicholls, 2011; Pesta & Gnaiger, 2012). The same protocol was used to perform respirometry in BMDM. Graph shows % of oxygen consumption in *pmol* $O_2/10^6$ *cells.*

*Isolated Mitochondria* - Mitochondria from liver or spleen (0.1-0.3 mg/mL) were incubated in the oxygraph chamber with an adaptation of MIR05 buffer: 0.5 mM EGTA, 3 mM $MgCl_2$, 20mM Taurine, 10 mM $KH_2PO4$, 20 mM Hepes, 110 mM D-sucrose, 1 g/L fatty acid–free BSA, 60 mM K-MES. The chamber final volume was 2.1mL. The chambers were closed right before the start of measurements. For isolated mitochondria, after a resting rate was obtained, respiration was induced by adding substrates for complex I or II, 5 mM glutamate/0.5 mM malate (GM) or 10 mM succinate, respectively. Other additions of reagents are indicated in the panel. The graph indicates the flow in pmol of $O_2$/mg of protein/second, and the respiration rates shown are subtracted from basal levels (mitochondria with no substrates). In Figure S3, a small adaptation of the protocol was performed based on (Kuznetsov et al., 2002) after the succinate step. We measured mitochondrial complex activities through different segments of the electron transport chain. After succinate addition, to activate respiration (CIII) we added 2.5 mM ADP. After this we inhibited complex I with 1 μM rotenone and complex III with 5 mM antimycin A (AA). This was followed by addition of the artificial substrates for complex IV (cytochrome c oxidase, COX), 0.5 mM TMPD, and 2 mM ascorbate. In this case, state 3 respiration (CIII) was determined by rates of (*ADP – AA)*, and CIV by (*TMPD/ascorbate – KCN)* rates. Based on that our measurements were: CI (NADH:ubiquinone oxidoreductase (rotenone sensitive)), CII ($FADH_2$: ubiquinone oxidoreductase), CIII (Ubiquinol-cytochrome *c* oxidoreductase (antimycin-sensitive)), CIV (cytochrome *c*- oxidoreductase (KCN-sensitive)).

Membrane potential was measured by using the fluorescence signal of the cationic dye, safranin-O. Liver mitochondria (0.2 mg protein/mL) were incubated in respiration buffer supplemented with 10 μM safranin O. Fluorescence was detected with an excitation wavelength of 495 nm and an emission wavelength of 586 nm (Spectra Max M5, Molecular Devices). Data are reported as percentage of maximal polarization induced by succinate.

**DNA extraction and Mitochondrial Content**

Total DNA was extracted from 1-2 x $10^6$ cells or 10-20 mg of liver tissue using DNeasy Blood & Tissue Kit (Qiagen). Mitochondrial content was assessed by real-time PCR analysis of the abundance of specific mitochondrial encoded genes relative to nuclear encoded genes using a CFX384 Real-Time System (Bio-Rad). For cells, analysis was performed by the SYBR Green method using primers for NADH dehydrogenase I (ND1) and Actin: (ND1: Forward *5'-TCA AAC TAC GCC CTG*

*ATC GG-3'* and Reverse *5'-GGA GAG GTT AAA GGA GCC ACT-3';* Actin: Forward *5'-TTC CTT CCT GGG CAT GGA GTC-3'* and Reverse *5'-AGA CAG CAC TGT GTT GGC GTA-3'*) (Amoêdo, et al, 2011). For mouse tissue, analysis was performed using commercially available Taqman probes for cytochrome c oxidase subunit (COX I), NADH dehydrogenase subunit 4 (ND4), and GAPDH, according to the manufacturer's instructions (Applied Biosystems, see table below). Mitochondrial copy number was calculated as ND1 relative to Actin for cells and COX1 or ND4 relative to GAPDH for tissue.

**Quantification of mRNA**

Omental fat was collected from healthy (BMI 32.8 ± 1.0 kg/m$^2$) kidney donors aged 30-68 years. The Protocol (10-005236) was approved by the Mayo Clinic Foundation Institutional Review Board for Human Research. Informed consent and consent to publish was obtained from all human subjects. RNA was isolated from human and mouse fat using the Trizol method, and from mouse liver and spleen using the RNeasy Plus Mini kit (Qiagen). cDNA was synthesized using QuantiTect Reverse Transcription kit (Qiagen). Quantitative real-time PCR was performed in triplicates using commercially available TaqMan gene expression probes (Applied Biosystems, see table below), according to the manufacturer's instructions, on a BioRad CFX384 thermal cycler. The relative mRNA abundance of target genes was calculated by the $2^{(-ddCq)}$ method (Livak and Schmittgen, 2001). The expression changes were calculated relative to control. Expression profiles for glucose metabolism and mitochondrial biogenesis pathways were analyzed using Qiagen RT2 Profiler PCR Arrays according to the manufacturer instructions (n=4 per group). RNA quality was assessed using an Agilent2100 Bioanalyzer.

**TaqMan Gene Expression Assays**

| | Gene Symbol | Probe ID |
|---|---|---|
| Mouse | *Cd38* | Mm01220906_m1 |
| | *Cox1* | Mm04225243_g1 |
| | *Nadk* | Mm00446804_m1 |
| | *Nampt* | Mm00451938_m1 |
| | *Naprt1* | Mm01205844_g1 |
| | *Nd4* | Mm04225294_s1 |
| | *Nmnat1* | Mm01257929_m1 |
| | *Nmnat2* | Mm00615393_m1 |
| | *Nmnat3* | Mm00513791_m1 |

| | | |
|---|---|---|
| | *Parp1* | Mm01321084_m1 |
| | *Parp2* | Mm00456462_m1 |
| | *Sirt1* | Mm00490758_m1 |
| | *Gapdh* | 4352932E |
| Human | *CD38* | Hs01120071_m1 |
| | *ND1* | Hs00159587_m1 |
| | *PARP1* | Hs00242302_m1 |
| | *NAMPT* | Hs00237184_m1 |
| | *ACTIN* | Hs03023943_g1 |

**SUPPLEMENTAL REFERENCES**


Amoêdo ND, Rodrigues MF, Pezzuto P, Galina A, da Costa RM, de Almeida FC, El-Bacha T, Rumjanek FD. Energy metabolism in H460 lung cancer cells: effects of histone deacetylase inhibitors. PLoS ONE. 2011;6(7).

Livak KJ, Schmittgen TD. Analysis of relative gene expression data using real-time quantitative PCR and the 2(-Delta Delta C(T)) Method. Methods. 2001;25:402–408.

Picard M, White K, Turnbull DM. Mitochondrial morphology, topology, and membrane interactions in skeletal muscle: a quantitative three-dimensional electron microscopy study. *Journal of Applied Physiology*. 2013;114(2):161-171.

Sisková Z, Mahad DJ, Pudney C, Campbell G, Cadogan M, Asuni A, O'Connor V, Perry VH. Morphological and functional abnormalities in mitochondria associated with synaptic degeneration in prion disease. Am J Pathol. 2010 Sep;177(3):1411-21**.**